

MAPPING THE EMISSION LOCATION OF THE CRAB PULSAR'S GIANT PULSES

ROBERT MAIN^{1,2,3}, MARTEN H. VAN KERKWIJK¹, UE-LI PEN^{2,4,3,5}, ALEXEI G. RUDNITSKII⁶, MIKHAIL V. POPOV⁶,
VLADIMIR A. SOGLASNOV⁶, MAXIM LYUTIKOV⁷

¹Department of Astronomy and Astrophysics, University of Toronto, 50 St. George Street, Toronto, ON M5S 3H4, Canada

²Canadian Institute for Theoretical Astrophysics, University of Toronto, 60 St. George Street, Toronto, ON M5S 3H8, Canada

³Dunlap Institute for Astronomy and Astrophysics, University of Toronto, 50 St George Street, Toronto, ON M5S 3H4, Canada

⁴Canadian Institute for Advanced Research, 180 Dundas St West, Toronto, ON M5G 1Z8, Canada

⁵Perimeter Institute for Theoretical Physics, 31 Caroline Street North, Waterloo, ON N2L 2Y5, Canada

⁶Astro Space Center, Lebedev Physical Institute, Russian Academy of Sciences, Profsoyuznaya ul. 84/32, Moscow, 117997 Russia

⁷Department of Physics, Purdue University, 525 Northwestern Avenue, West Lafayette, IN 47907-2036, USA

ABSTRACT

The Crab pulsar has striking radio emission properties, with the two dominant pulse components – the main pulse and the interpulse – consisting entirely of giant pulses. The emission is scattered in both the Crab nebula and the interstellar medium, causing multi-path propagation and thus scintillation. We study the scintillation of the Crab's giant pulses using phased Westerbork data at 1668 MHz. From correlations of the giant pulse spectra, we find that the main pulse and the interpulse are significantly offset in time and frequency. This suggests that they arise in physically distinct regions, which are, assuming the scattering takes place in the nebular filaments, separated by about a light cylinder radius (as projected on the sky). With further VLBI and multi-frequency data, it should be possible to measure both the distance to the scattering screens and the physical separation between the pulse components.

1. THE UNUSUAL PROPERTIES OF THE CRAB PULSAR

The Crab pulsar is one of the most unusual radio pulsars, and has been the subject of much observational and theoretical research (for a review, see [Eilek & Hankins 2016](#)). The two dominant components to its radio pulse profile, the main pulse and the low-frequency interpulse (simply referred to as the interpulse for the remainder of this paper), appear to be comprised entirely of randomly occurring giant pulses – extremely short and bright pulses of radio emission showing structure down to ns timescales and reaching intensities over a MJy ([Hankins & Eilek 2007](#)). Only the fainter components of the pulse profile – such as the precursor (to the main pulse) – are similar to what is seen for regular radio pulsars.

The main pulse and interpulse are aligned within 2 ms with X-ray and γ -ray components ([Moffett & Hankins 1996](#); [Abdo et al. 2010](#)). Since pair production strongly absorbs γ -ray photons inside the magnetosphere, this suggests both components arise far from the neutron-star surface, with possible emission regions being the various magnetospheric “gaps” ([Romani & Yadigaroglu 1995](#); [Muslimov & Harding 2004](#); [Qiao et al. 2004](#); [Istomin 2004](#)) or regions outside the light cylinder ([Philippov et al. 2015](#)). While similar in their overall proper-

ties, the main pulse and interpulse have differences in detail. In particular, the interpulse has a large scatter in its dispersion measure compared to the main pulse, possibly suggesting that it is observed through a larger fraction of the magnetosphere ([Eilek & Hankins 2016](#)). In addition, it appears shifted in phase and shows “banding” in its power spectra above 4 GHz, with spacing proportional to frequency ([Hankins & Eilek 2007](#)).

The Crab pulsar, like many pulsars, exhibits scintillation from multi-path propagation of its radio emission. The scattering appears to include both a relatively steady component, arising in the interstellar medium, and a highly variable one, originating in the the Crab nebula itself, with the former responsible for the angular and the latter for (most of) the temporal broadening ([Rankin & Counselman 1973](#); [Vandenberg 1976](#); [Popov et al. 2017](#); [Rudnitskii et al. 2017](#)). The proximity of the nebular scattering screen to the pulsar implies that, as seen from the pulsar, the screen extends a much larger angle than would be the case if it were far away (for a given scattering time). Therefore, the scintillation pattern is sensitive to small spatial scales, of order ~ 2000 km at our observing frequency (see Sect. 4.1), comparable to the light-cylinder radius $r_{\text{LC}} \equiv cP/2\pi \simeq 1600$ km.

The high spatial resolving power also implies that,

for given relative velocity between the pulsar and the screen, the scintillation timescale is short. Indeed, from the scintillation properties of giant pulses, [Cordes et al. \(2004\)](#) infer a de-correlation time of ~ 25 s at 1.4 GHz. [Karuppusamy et al. \(2010\)](#) compare the scintillation of pulses within a single pulse rotation, finding that main pulses weakly correlate with interpulses. In this paper, we compare the scintillation structure of the main pulse and the interpulse in more detail. We find that there are significant differences, which indicate that, as projected on the sky, the locations at which their emission originate differ on the scale of the light cylinder.

2. OBSERVATIONS AND DATA REDUCTION

We analyse 6 hours of phased Westerbork data that were taken as part of a RadioAstron observing run on 2015, January 10–11 ([Popov et al. 2017](#)). The data cover the frequency range of 1652–1684 MHz, consisting of both circular polarizations in two contiguous 16 MHz channels, recorded using standard 2-bit Mark 5B format. A large phased array like Westerbork is particularly beneficial in studies of the Crab pulsar, as it helps to resolve out the Crab nebula, effectively reducing the system temperature from 830 Jy (for the integrated flux at 1.7 GHz) to 165 Jy ([Popov et al. 2017](#)).

To search for giant pulses, we coherently dedispersed¹ the data from the two channels to a common reference frequency, and summed the power from both channels and both polarizations in $8 \mu\text{s}$ bins. We flagged peaks above 6σ , corresponding to ~ 45 Jy, as giant pulses, finding in 29332 events, i.e., a rate of $\sim 1.6 \text{ s}^{-1}$. We show the detected pulses in [Fig. 1](#), along with the folded profile.

3. SCINTILLATION PROPERTIES

With the phased Westerbork array, our pulse detection rate is sufficiently high that it becomes possible to compute a traditional dynamic spectrum by summing intensities as a function of time. We do this first below, as it gives an immediate qualitative view of the scintillation. A more natural choice for pulses which occur randomly in time, however, is to parametrize variations as a function of Δt , the time separation between pulses ([Cordes et al. 2004](#); [Popov et al. 2017](#)). Hence, we continue by constructing correlation functions of the spectra, as functions of both time and frequency offset.

3.1. The Dynamic Spectrum of the Main Pulse

During our observation, the scattering time in the Crab was relatively small, smaller than the intrinsic

duration of the pulses, such that we can resolve scintillation patterns in frequency. We can thus construct the dynamic spectrum $I(t, \nu)$ by simply summing giant pulse spectra, normalizing each time bin by the total flux within that bin. While there will still be structure in the dynamic spectrum owing to the intrinsic time structure of the giant pulses ([Cordes et al. 2004](#)), any features in frequency which correlate in time should only be associated with scintillation. We show a 20 minute segment of the dynamic spectrum in [Figure 2](#). While noisy, the dynamic spectrum shows scintillation features. They are resolved by our time and frequency bin sizes of 4 s and 250 kHz, respectively, but only by a few bins, suggesting that the scintillation timescale and bandwidth are larger than our bin sizes by a factor of a few.

3.2. Correlation Functions

The correlation function between two spectral intensity streams $I_1(t, \nu)$ and $I_2(t, \nu)$ can be written as,

$$R(\Delta t, \Delta \nu) = \frac{\langle (I_1(t, \nu) - \mu_1)(I_2(t + \Delta t, \nu + \Delta \nu) - \mu_2) \rangle}{\sigma_1 \sigma_2}, \quad (1)$$

where Δt and $\Delta \nu$ are offsets in time and frequency, μ_1 and μ_2 are averages of I_1 and I_2 over time and frequency, and σ_1 and σ_2 estimates of the standard deviation.

To infer the scintillation bandwidth and timescale, one usually uses the auto-correlation of the dynamic spectrum, but for pulses randomly spaced in time, it is easier to calculate covariances for pulse pairs and then bin by time separation Δt ([Cordes et al. 2004](#)). To do this, we begin by selecting only pulses above 16σ – which implies that they have a signal-to-noise ratio of $\gtrsim 1$ in each 125 kHz channel. We then correlate each pulse pair, taking care to account for the contributions of noise to variance in the spectra (see [Appendix A](#)), giving an estimate of $R(\Delta t, \Delta \nu)$ for a single value of Δt , the time separation of the pulses. We then sum these correlated spectra in equally spaced bins of Δt to construct our average correlation function. In [Fig. 3](#), we show the result, both for correlations between main pulse pairs and for correlations between main pulse and interpulse pairs (there are insufficient giant pulses associated with the interpulse to calculate a meaningful correlation function from those).

The main pulse spectra decorrelate on a scale of $\Delta \nu = 1.18 \pm 0.01$ MHz in frequency, and on a scale of $\tau = 9.0 \pm 0.1$ s in time.² The time scale is somewhat shorter than the value of 25 ± 5 s found at 1.475 MHz by [Cordes et al. \(2004\)](#), even accounting for the difference in

¹ Using a dispersion measure of $56.7716 \text{ pc cm}^{-3}$ appropriate for our date (taken from <http://www.jb.man.ac.uk/~pulsar/crab.html>; [Lyne et al. 1993](#)). We took care to read sufficient extra data to avoid de-dedispersion wrap-around.

² We adopt the usual convention, defining $\Delta \nu$ and τ as the values where the correlation function drops to $1/2$ and $1/e$ respectively.

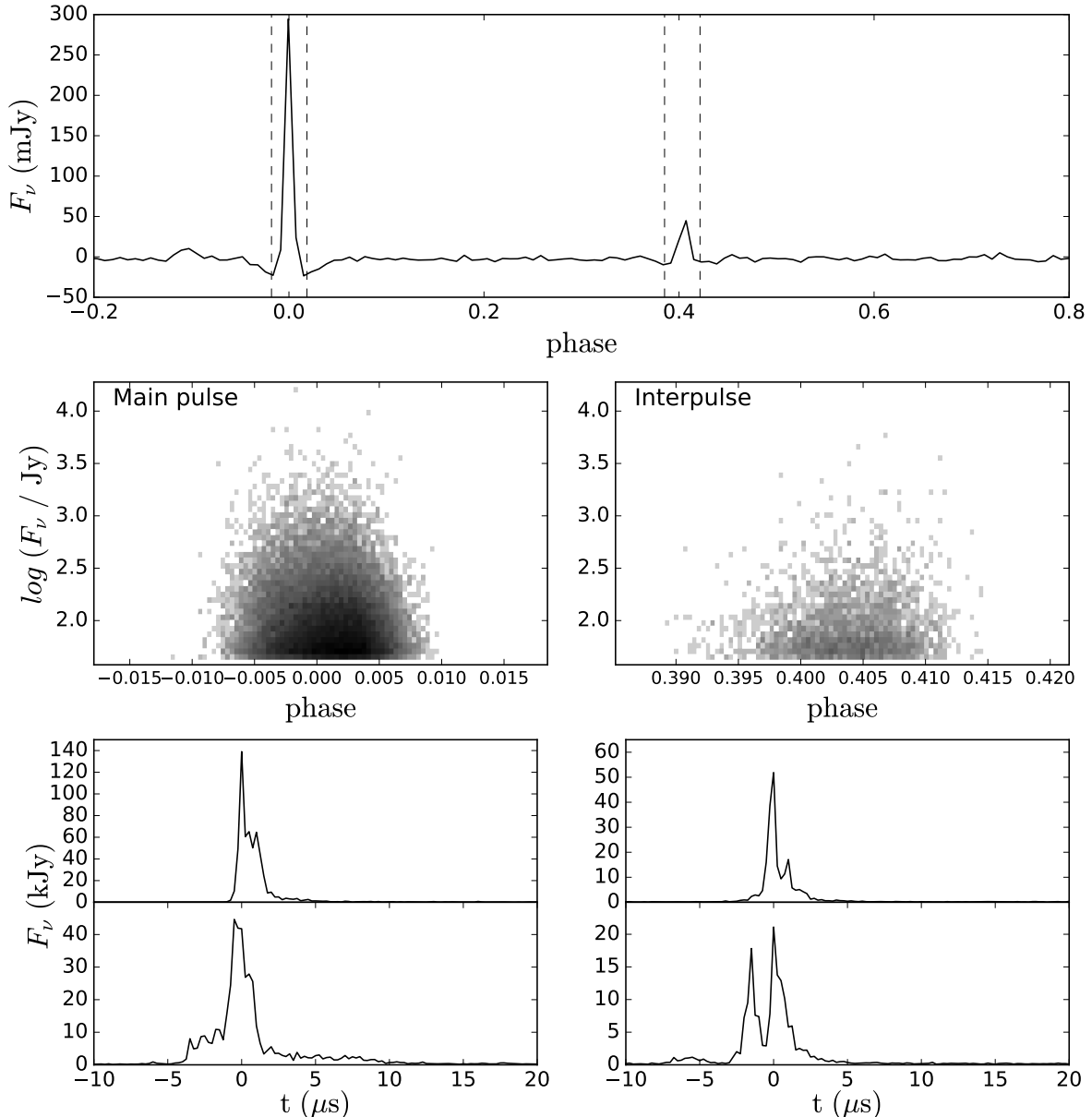


Figure 1. *Top:* Average pulse profile across our observation, derived by folding the dedispersed data in 128 phase bins. *Middle panels:* Flux density of all giant pulses detected around the main pulse and the interpulse, as measured in the $8 \mu\text{s}$ bins used to search for them. Note that since the giant pulses arrive only sporadically, the folded profile has far lower flux than the giant pulses. The dips around the main and interpulse in the folded profile are an artefact from the 2-bit digitization. *Bottom Panels:* Pulse profiles of the two brightest main pulses (*left*) and inter-pulses (*right*) in 250 ns bins. Note the large intrinsic differences between pulse profiles.

frequency (for $\tau \propto \nu^{-4}$, our measurement corresponds to $5.7 \pm 0.1 \text{ s}$ at 1.475 GHz). Differences are expected for observations at different epochs, however, as the scattering in the nebula is highly variable (Rankin & Counselman 1973; Lyne & Thorne 1975; Isaacman & Rankin 1977; Rudnitskii et al. 2017, and sometimes showing “echoes”, e.g., Backer et al. 2000; Lyne et al. 2001).

Attention should be paid to intrinsic time structure of individual giant pulses and its influence on the scintillation spectra. It was shown that such influence decreases

when giant pulse spectra in different polarization channels are correlated (Kondratiev et al. 2007). However, such influence in this case is not completely excluded; the shot noise structure of giant pulses which results in the intrinsic fine frequency structure is correlated between different polarizations (e.g. Eilek & Hankins 2016). This appears to be why the decorrelation bandwidth obtained in this paper significantly differs from what was calculated in Popov et al. (2017) for the same dataset, who auto-correlate giant pulse spectra between

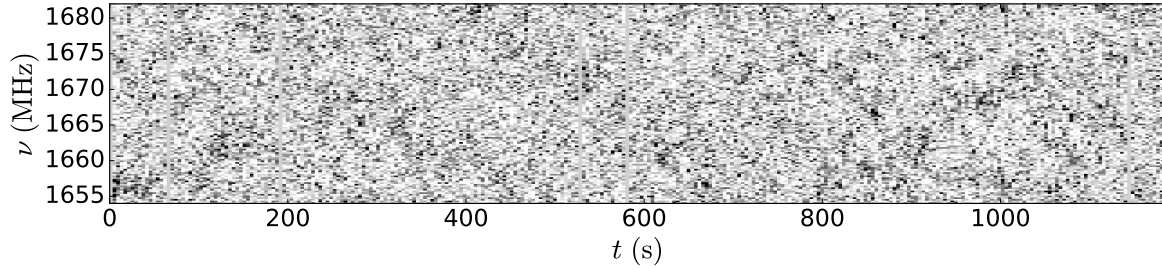


Figure 2. Part of the dynamic spectrum inferred from the main pulse by summing individual giant pulse spectra at 250 kHz resolution in 4s bins. The total flux in each time bin was normalized to remove the effects of variable pulse brightness (which otherwise would dominate the spectrum). The random occurrence of giant pulses and their variable flux means that the noise properties of the time bins are heterogeneous, and that some bins have no flux.

their left and right circular polarizations. If we adopt the cutoff of $\text{SN} > 22$ as in [Popov et al. \(2017\)](#), correlate left and right circular polarizations and fit a single exponential, then we measure $\Delta\nu = 0.42$ MHz, closer to their value. However, a two-exponential fit is a better fit to the data, giving two distinct scales of $\Delta\nu_1 = 0.98$ MHz, $\Delta\nu_2 = 0.16$ MHz; the above explanation is consistent with our results if the small bandwidth $\Delta\nu$ is caused by intrinsic pulse structure, and the wide bandwidth $\Delta\nu$ is the scintillation bandwidth.

In [Fig. 3](#), one sees that the main pulse to interpulse correlation function is different from the main-pulse autocorrelation, being offset in time and frequency by about -3 s and -0.5 MHz, respectively, and having a lower maximum correlation. To quantify the significance of these differences, we use simulated cross-correlations. For these, since we have many more giant pulses during the main pulse than the interpulse, we simply take 528 random main pulses (the number of interpsuls above 16σ) and correlate these with the other 6401 main pulses. We repeat this 10000 times, and fit each subset with a 2D Gaussian, allowing for offsets in time and frequency Δt_0 and $\Delta\nu_0$. Comparing these with the value fit to the interpulse to main-pulse correlations (see side panels in [Fig. 3](#)), the differences are significant: none of the simulated data sets have larger Δt_0 or $\Delta\nu_0$, or as small an amplitude.

The reduced amplitude makes it somewhat difficult to estimate uncertainties on time and frequency offsets. We estimate them by scaling the standard deviations from the simulations by the ratio of the main simulated amplitude to the observed one, yielding $\Delta t_0 = -3.0 \pm 0.5$ s and $\Delta\nu_0 = -0.52 \pm 0.06$ MHz.

4. RAMIFICATIONS

4.1. Spatial Resolution of Scattering Screen

The size and location of the scattering screen is not precisely known, but a model in which the temporal scattering occurs in the Crab nebula is favored by VLBI measurements showing the visibility amplitude is con-

stant through the scattering tail ([Vandenberg et al. 1976](#)) as well as the short scintillation timescale ([Cordes et al. 2004](#)). The geometric time delay is

$$\tau = \frac{\theta^2 d_{\text{eff}}}{2c} \quad \text{with} \quad d_{\text{eff}} = \frac{d_{\text{psr}} d_{\text{scr}}}{d_{\text{psr}} - d_{\text{scr}}}, \quad (2)$$

where θ is the angle the screen extends to as seen from Earth, and d_{psr} and d_{scr} are the distances to the pulsar and the screen, respectively. The scattering screen can be seen as a lens, with physical size $D = \theta d_{\text{scr}}$ and corresponding angular resolution λ/D , giving a physical resolution at the pulsar of $\Delta x = (d_{\text{psr}} - d_{\text{scr}})\lambda/\theta d_{\text{scr}}$, or, in terms of the scattering time τ ,

$$\Delta x = \lambda \left(\frac{d_{\text{psr}} - d_{\text{scr}}}{2c\tau} \frac{d_{\text{psr}}}{d_{\text{scr}}} \right)^{1/2}. \quad (3)$$

Assuming the scattering is dominated by the nebula, we have $d_{\text{scr}} \simeq d_{\text{psr}}$ and hence for the known scattering time $\tau \simeq 160$ ns (from $\tau = 1/2\pi\Delta\nu$, $\Delta\nu \approx 1$ MHz), the dominant unknown is the distance between the pulsar and the screen.

Since scattering requires relatively large differences in (electron) density, it cannot happen inside the pulsar-wind filled interior of the Crab nebula, which must have very low density. For a reasonable bulk magnetic field of 10^{-4} G, the emitting electrons are relativistic, with $\gamma \sim 10^6$. The radio emitting electrons have a density of $n_e \approx 10^{-5} \text{ cm}^{-3}$ ([Shklovsky 1957](#)), implying that the refractive index deviates from unity by a tiny amount,

$$\Delta n \approx \left(\frac{\omega_p}{\omega_R} \right)^2 \sim 10^{-32}, \quad (4)$$

where $\omega_p = (4\pi e^2 n_e / \gamma m_e)^{1/2}$ is the plasma frequency, and ω_R is the observed radio frequency.

Instead, the only plausible location for the temporal scattering is in the optically emitting filaments in the Crab Nebula. These filaments develop due to the Rayleigh Taylor instability: as the pulsar wind pushes on the shell material, the contact discontinuity accelerates ([Chevalier 1977](#)) leading to the RT instability and formation of filaments ([Porth et al. 2014](#)).

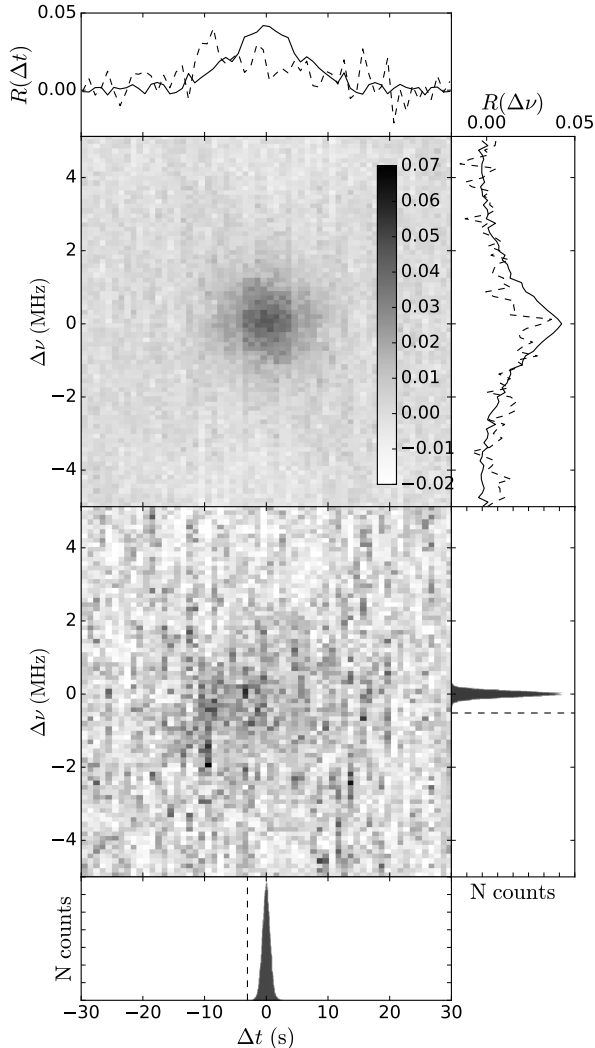


Figure 3. *Images:* Cross-correlations $R(\Delta t, \Delta\nu)$ of pulse dynamic spectra, between giant pulses in the main pulse with themselves (*top*) and with giant pulses in the interpulse (*bottom*). The correlation between main-pulse giant pulses is symmetric by construction (i.e., $R(\Delta t, \Delta\nu) = R(-\Delta t, -\Delta\nu)$), but this is not the case for the correlation between interpulse and main pulse. The offsets likely reflect a different physical location of the main pulse and interpulse emission regions (see section 4.1). *Top and top-right:* a 5-bin wide average of main pulse (solid line) and interpulse (dashed line) correlations through the best fit Δt , $\Delta\nu$, respectively. *Bottom and bottom-right Panels:* Comparison of the best-fit offsets Δt_0 and $\Delta\nu_0$ found by fitting a two-dimensional Gaussian to the interpulse, main-pulse correlation function with simulated correlation functions constructed from randomly drawn sets of giant pulses from the main pulse (with the same size as that available for the interpulse). None of these have offsets as large as the ones observed.

With 3-dimensional models fit to spectroscopic optical data of the Crab Nebula, Lawrence et al. (1995) find the filaments reside in the range 0.3–0.75 pc when using a nominal pulsar distance of 2 kpc (given the full range

of distances, $1.4 \lesssim d_{\text{psr}} \lesssim 2.7$ kpc from Trimble 1973, implying filaments in the range 0.2–1 pc). Assuming $d_{\text{psr}} - d_{\text{scr}} \simeq 0.5$ pc, then $\Delta x \simeq 2300$ km (for the full range of possibilities $1400 \lesssim \Delta x \lesssim 3200$ km). Thus, the resolution of the scattering screen is comparable to the light-cylinder radius of the Crab pulsar, $R_{\text{LC}} \equiv cP/2\pi = 1600$ km.

From Fig. 3, one sees that at zero time delay the correlation between interpulse and main pulse has become quite small. This suggests that the emission locations are separated by of order one resolution element of the screen, or, equivalently, of order the light cylinder radius. The larger correlation at larger delay implies that the interpulse does cross a similar position relative to the screen about 3 s later. We could turn this into a physical separation given a relative velocity between the pulsar and the screen. Unfortunately, this is not known, though we can set limits from the proper motion. The proper motion of the Crab pulsar relative to its local standard of rest is measured to be 12.6 ± 6.2 mas/yr in direction 160 ± 30 deg, where the uncertainties attempt to account for the uncertainty in the velocity of its progenitor (Kaplan et al. 2008), and, therewith, of the nebular material. At an assumed distance of 2 kpc, the implied relative velocity of ~ 120 km/s suggests a projected separation between the interpulse and main pulse emission regions of ~ 360 km.

4.2. Fully Measuring the Separation

A major uncertainty in the estimate of the spatial separation between the main pulse and the interpulse is the geometry of the lens. From studies of the scintillation in other pulsars, the scattering screens in the interstellar medium are known to be highly anisotropic, as demonstrated most dramatically by the VLBI observations of Brisken et al. (2010). If the same holds for the nebular scattering screens, this implies that our resolution elements are similarly anisotropic. Since the orientation relative to the proper motion is unknown, the physical distance between the main and interpulse regions could be either smaller or larger than our estimate above. Since the scattering varies with time, it may be possible to average out these effects.

Furthermore, all values relating to the scattering screen include the uncertain distance to the Crab pulsar, suggesting that a parallax distance would improve our constraints. In addition, the rough location of the scattering in the filaments is a physical argument, and would be greatly improved through a direct measurement.

The distance to the screen(s) can be constrained through VLBI and through scintillation measurements across frequency. VLBI at space-ground baselines (Rudnitskii et al. 2016) or at low frequencies (Kirsten et al., in prep.) can help constrain the angular size of the scat-

tering in the interstellar medium. This in turn can constrain the size of the nebular screen; the visibility amplitudes will only decrease below 1 when the scattered image of the pulsar is not point-like to the interstellar screen. In addition, two scattering screens will impart two distinct scattering times only when they do not resolve each other (Masui et al. 2015). The transition frequency for the two scintillation timescales to become apparent in the spectra will give a size measurement of the nebular screen.

Applying this same analysis across different frequen-

cies, or in times of different scattering in the nebula will also help to quantify both the separation of the main pulse and interpulse, and the size of the emitting regions of both components.

We thank Judy Xu who attempted the initial 1D correlation function of giant pulses, and Rebecca Lin who reproduced our results and noticed errors in early version of this work. We made use of NASA's Astrophysics Data System and SOSCIP Consortiums Blue Gene/Q computing platform.

Software: Astropy (Astropy Collaboration et al. 2013)

REFERENCES

- Abdo, A. A., Ackermann, M., Ajello, M., et al. 2010, *ApJ*, 708, 1254
- Astropy Collaboration, Robitaille, T. P., Tollerud, E. J., et al. 2013, *A&A*, 558, A33
- Backer, D. C., Wong, T., & Valanju, J. 2000, *ApJ*, 543, 740
- Bhat, N. D. R., Cordes, J. M., & Chatterjee, S. 2003, *ApJ*, 584, 782
- Brisken, W. F., Macquart, J.-P., Gao, J. J., et al. 2010, *ApJ*, 708, 232
- Chevalier, R. A. 1977, *ARA&A*, 15, 175
- Cordes, J. M., Bhat, N. D. R., Hankins, T. H., McLaughlin, M. A., & Kern, J. 2004, *ApJ*, 612, 375
- Eilek, J. A., & Hankins, T. H. 2016, *Journal of Plasma Physics*, 82, 635820302
- Gelfand, J. D., Slane, P. O., & Zhang, W. 2009, *ApJ*, 703, 2051
- Hankins, T. H., & Eilek, J. A. 2007, *ApJ*, 670, 693
- Isaacman, R., & Rankin, J. M. 1977, *ApJ*, 214, 214
- Istomin, Y. N. 2004, in *IAU Symposium*, Vol. 218, Young Neutron Stars and Their Environments, ed. F. Camilo & B. M. Gaensler, 369
- Kaplan, D. L., Chatterjee, S., Gaensler, B. M., & Anderson, J. 2008, *ApJ*, 677, 1201
- Karuppusamy, R., Stappers, B. W., & van Straten, W. 2010, *A&A*, 515, A36
- Kondratiev, V. I., Popov, M. V., Soglasnov, V. A., et al. 2007, *Astronomical and Astrophysical Transactions*, 26, 585
- Kuzmin, A., Losovsky, B. Y., Jordan, C. A., & Smith, F. G. 2008, *A&A*, 483, 13
- Lawrence, S. S., MacAlpine, G. M., Uomoto, A., et al. 1995, *AJ*, 109, 2635
- Lyne, A. G., Pritchard, R. S., & Graham-Smith, F. 1993, *MNRAS*, 265, 1003
- . 2001, *MNRAS*, 321, 67
- Lyne, A. G., & Thorne, D. J. 1975, *MNRAS*, 172, 97
- Lyutikov, M. 2007, *MNRAS*, 381, 1190
- Main, R., van Kerkwijk, M., Pen, U.-L., Mahajan, N., & Vanderlinde, K. 2017, *ApJL*, 840, L15
- Masui, K., Lin, H.-H., Sievers, J., et al. 2015, *Nature*, 528, 523
- Moffett, D. A., & Hankins, T. H. 1996, *ApJ*, 468, 779
- Muslimov, A. G., & Harding, A. K. 2004, *ApJ*, 606, 1143
- Pen, U.-L., Macquart, J.-P., Deller, A. T., & Brisken, W. 2014, *MNRAS*, 440, L36
- Philippov, A. A., Cerutti, B., Tchekhovskoy, A., & Spitkovsky, A. 2015, *ApJL*, 815, L19
- Popov, M. V., Rudnitskii, A. G., & Soglasnov, V. A. 2017, *Astronomy Reports*, 61, 178
- Popov, M. V., & Stappers, B. 2007, *A&A*, 470, 1003
- Porth, O., Komissarov, S. S., & Keppens, R. 2014, *MNRAS*, 443, 547
- Qiao, G. J., Lee, K. J., Wang, H. G., Xu, R. X., & Han, J. L. 2004, *ApJL*, 606, L49
- Rankin, J. M., & Counselman, III, C. C. 1973, *ApJ*, 181, 875
- Romani, R. W., & Yadigaroglu, I.-A. 1995, *ApJ*, 438, 314
- Rudnitskii, A. G., Karuppusamy, R., Popov, M. V., & Soglasnov, V. A. 2016, *Astronomy Reports*, 60, 211
- Rudnitskii, A. G., Popov, M. V., & Soglasnov, V. A. 2017, *Astronomy Reports*, 61, 393
- Shklovsky, I. S. 1957, in *IAU Symposium*, Vol. 4, Radio astronomy, ed. H. C. van de Hulst, 201
- Slane, P. 2017, *ArXiv e-prints*, arXiv:1703.09311
- Trimble, V. 1973, *PASP*, 85, 579
- Vandenberg, N. R. 1976, *ApJ*, 209, 578
- Vandenberg, N. R., Clark, T. A., Erickson, W. C., Resch, G. M., & Broderick, J. J. 1976, *ApJ*, 207, 937
- Weatherall, J. C. 1998, *ApJ*, 506, 341
- Zhuravlev, V. I., Popov, M. V., Kondrat'ev, V. I., et al. 2011, *Astronomy Reports*, 55, 724

APPENDIX

A. CORRECTING NOISE BIASES IN THE CORRELATION COEFFICIENT

The correlation coefficient between two pulse intensity spectra $I_{1,2}(\nu)$ can be generally defined as,

$$R(I_1(\nu), I_2(\nu)) = \frac{\langle (I_1(\nu) - \mu_1)(I_2(\nu) - \mu_2) \rangle}{\sigma_1 \sigma_2}, \quad (\text{A1})$$

where $\langle \dots \rangle$ indicates an average over frequency, and μ and σ are measures of the average and variations around it, respectively. Typically, one chooses $\mu_P = \langle I_P(\nu) \rangle$ and $\sigma_P = s_P \equiv \langle (I_P - \mu_P)^2 \rangle^{1/2}$ so that, in the absence of noise, $R = 1$ for two pulses with intrinsically identical frequency structure. In the presence of some measurement noise σ_n ,

one could approximate $\sigma_P^2 = s_P^2 - \sigma_n^2$, but this holds only for normally-distributed noise, not for our case of intensity spectra.

Here, we derive an expression valid for our case, where we wish to ensure that $R = 1$ for two pulses that are sufficiently short that we can approximate them as delta functions, and that are affected by the interstellar medium the same way, i.e., have the same impulse transfer function $g(t)$. In that case, the measured electric field of a giant pulse is,

$$E_P(\nu) = A_P g(\nu) + n(\nu), \quad (\text{A2})$$

where A_P is the amplitude of the pulse's delta function in the Fourier domain, and $g(\nu)$ and $n(\nu)$ the Fourier transforms of the impulse response function and the measurement noise, respectively. The measured intensity is then

$$I_P(\nu) = E_P^2(\nu) = A_P^2 g^2(\nu) + n^2(\nu) + 2A_P |g(\nu)| |n(\nu)| \cos(\Delta\phi(\nu)), \quad (\text{A3})$$

where $\Delta\phi(\nu)$ is the phase difference between $n(\nu)$ and $g(\nu)$.

The expectation value for the average is,

$$\mu_P = \langle I_P \rangle = A_P^2 \langle g^2 \rangle + \langle n^2 \rangle, \quad (\text{A4})$$

where we have dropped the dependencies on frequency for brevity, and used that the cross term averages to zero since $\langle \cos(\Delta\phi) \rangle = 0$. Hence, the expectation value for standard deviation is,

$$s_P^2 = A^4 [\langle (g^4) - \langle g^2 \rangle^2 \rangle + \langle n^4 \rangle - \langle n^2 \rangle^2 + 4A^2 \langle g^2 n^2 \cos^2(\Delta\phi) \rangle], \quad (\text{A5})$$

where we have again omitted terms that average to zero. The last term does not average to zero because of the squaring: it reduces to $2A_P^2 \langle g^2 \rangle \langle n^2 \rangle$, since g and n are independent and $\langle \cos^2(\Delta\phi) \rangle = 1/2$.

For two pulses affected by the same $g(\nu)$, and assuming that both g and n are roughly normally distributed in their real and imaginary parts, so that g^2 and n^2 are distributed as χ^2 distributions for 2 degrees of freedom, and $\langle g^4 \rangle = 2\langle g^2 \rangle^2$ (and the same for n), the numerator of R becomes $A_1^2 A_2^2 \langle g^2 \rangle^2$. Thus, for an unbiased estimate of R , we need to estimate $\sigma_P = A_P \langle g^2 \rangle$. We can do this by also measuring the properties of the background, which, if it is dominated by measurement noise with the same properties as the pulse, has $\mu_B = \langle n^2 \rangle$ and $s_B^2 = \langle n^4 \rangle + \langle n \rangle^2$. With this, it follows that to make estimates of R free of noise bias, we should use,

$$\sigma_P^2 = s_P^2 - s_B^2 - 2(\mu_P - \mu_B)\mu_B. \quad (\text{A6})$$

To test the above, we simulated identical giant pulses with different noise in the manner described in [Main et al. \(2017\)](#). We find that using the above estimates, the correlation coefficients between these pulses indeed average to unity when the impulse response functions are the same.